# Low-*n* shear Alfvén spectra in axisymmetric toroidal plasmas

C. Z. Cheng, and M. S. Chance

Citation: The Physics of Fluids **29**, 3695 (1986); doi: 10.1063/1.865801
View online: https://doi.org/10.1063/1.865801
View Table of Contents: https://aip.scitation.org/toc/pfl/29/11
Published by the American Institute of Physics

# Low-$n$ shear Alfvén spectra in axisymmetric toroidal plasmas

C. Z. Cheng and M. S. Chance
*Princeton Plasma Physics Laboratory, P. O. Box 451, Princeton, New Jersey 08544*

(Received 31 October 1985; accepted 4 August 1986)

In toroidal plasmas, the toroidal magnetic field is nonuniform over a magnetic surface and causes coupling of different poloidal harmonics. It is shown both analytically and numerically that the toroidicity not only breaks up the shear Alfvén continuous spectrum, but also creates new, discrete, toroidicity-induced shear Alfvén eigenmodes with frequencies inside the continuum gaps. Potential applications of the low-$n$ toroidicity-induced shear Alfvén eigenmodes on plasma heating and instabilities are addressed.

## I. INTRODUCTION

Shear Alfvén continuous spectra have been extensively studied[1–10] for both cylindrical and toroidal plasmas by using the ideal magnetohydrodynamic (MHD) model. The understanding of the shear Alfvén continuous spectra in toroidal geometries is essential for plasma heating by means of the resonant absorption of Alfvén waves with frequencies lying within the continuous spectra. A great deal of attention has been placed on the toroidal coupling effects[8–10] because a nonuniform toroidal magnetic field over a magnetic surface can cause interactions among the neighboring poloidal harmonics and can break up the shear Alfvén continuous spectrum with gaps. However, a complete understanding of the stable shear Alfvén spectra for axisymmetric toroidal plasmas is still not achieved. In this paper we will thoroughly examine the stable shear Alfvén spectra and show that the toroidal coupling effects not only break up the shear Alfvén continuous spectrum, but also result in discrete, global, toroidicity-induced shear Alfvén eigenmodes with frequencies inside the continuum gaps. The existence of the discrete, global toroidicity-induced shear Alfvén eigenmodes suggest a new and more efficient Alfvén wave heating scheme. In addition, instabilities of the discrete toroidicity-induced eigenmodes can be excited by tapping the free energy of energetic particles associated with the plasma inhomogeneities through wave–particle resonances. Our analysis will be limited to low-$n$ modes, where $n$ is the toroidal mode number. For high-$n$ modes, extensive analytical and numerical solutions[10] have been obtained for the shear Alfvén spectra by solving the high-$n$ ballooning mode equation.

Recent investigations[11–13] of shear Alfvén waves in cylindrical plasmas have also indicated existence of discrete stable global Alfvén eigenmodes[11,12] with frequencies below the minimum of the Alfvén continuum for a given toroidal mode number $n$ and a poloidal mode number $m$, i.e., $0<\omega^2<\min[\omega_A^2(r)]$, where $\omega_A^2(r)=(m-nq)^2V_A^2/q^2R^2$, $m$ and $n$ have different signs, $q$ is the safety factor, $R$ is the major radius, and $V_A$ is the Alfvén speed. These modes represent stable kink modes and exist only under certain well-defined conditions. They are different from our discrete toroidicity-induced modes and are called "cylindrical global Alfvén waves." In toroidal geometries, the cylindrical global Alfvén waves have singular mode structures with frequencies embedded in continuous spectra due to toroidal couplings of different poloidal harmonics. We do not discuss these modes here.

In Sec. II, we formulate the ideal MHD eigenmode equations in a new form to provide for a better physical representation. This forms the basis of our numerical solutions. Analytical and numerical analyses of the breakups of the continuous spectrum caused by toroidal coupling effects are presented in Sec. III. In Sec. IV, the numerical solutions of the discrete, global, low-$n$ toroidicity-induced shear Alfvén eigenmodes are shown, and the analytical theories are performed on the reduced MHD equations in a low-$\beta$ limit. Finally, a discussion of the major results and some implications for plasma heating and instabilities related to the low-$n$ toroidicity-induced shear Alfvén modes are given in Sec. V.

## II. FORMULATION

We consider linearized ideal MHD operations in stationary MHD equilibria satisfying

$$\mathbf{J}\times\mathbf{B}=\nabla P,\quad \nabla\times\mathbf{B}=\mathbf{J},\quad \text{and } \nabla\cdot\mathbf{B}=0, \tag{1}$$

where $\mathbf{J}$, $\mathbf{B}$, and $P$ are the equilibrium current, magnetic field, and plasma pressure, respectively. In terms of the straight field line flux coordinate system $(\psi,\theta,\zeta)$, the axisymmetric toroidal equilibrium magnetic field can be written as

$$\mathbf{B}=\nabla\zeta\times\nabla\psi+q(\psi)\nabla\psi\times\nabla\theta, \tag{2}$$

where $q$ is the safety factor, $2\pi\psi$ is the poloidal flux within a magnetic surface, $\theta$ is a generalized poloidal angle with a period of $2\pi$, and $\zeta$ is a generalized toroidal angle with a period of $2\pi$. If $P(\psi)$ and $g(\psi)$ are specified, an axisymmetric toroidal equilibrium can be determined numerically by solving the Grad–Shafranov equation

$$\Delta^*\psi\equiv X^2\nabla\cdot(X^{-2}\nabla\psi)=-(X^2P'+gg'). \tag{3}$$

In this paper, a prime denotes the partial derivative with respect to $\psi$. Let $\boldsymbol{\xi}$, $\mathbf{b}$, and $p$, be the perturbed plasma displacement, magnetic field, and plasma pressure, respectively. With the time dependence $\boldsymbol{\xi}(\mathbf{x},t)=\boldsymbol{\xi}(\mathbf{x})e^{-i\omega t}$, the linearized ideal MHD equations are given by

$$p_1+\boldsymbol{\xi}\cdot\nabla P+\gamma_s P\nabla\cdot\boldsymbol{\xi}=0, \tag{4}$$

$$\rho\omega^2\boldsymbol{\xi}=\nabla p_1+\mathbf{b}\times(\nabla\times\mathbf{B})+\mathbf{B}\times(\nabla\times\mathbf{b}), \tag{5}$$

and

$$\mathbf{b}=\nabla\times(\boldsymbol{\xi}\times\mathbf{B}), \tag{6}$$

 0031-9171/86/113695-07$01.90  

where $\gamma_s = 5/3$ is the ratio of specific heats and $\rho$ the plasma density. Equations (4)–(6) can further be simplified by employing the variables $\nabla\cdot\xi$, $\xi_s$, $\xi_\psi$, and $P_1$, where $\xi_s = \xi\cdot(\mathbf{B}\times\nabla\psi)/|\nabla\psi|^2$ is the surface displacement, $\xi_\psi = \xi\cdot\nabla\psi$ is the radial displacement, and $P_1 = p_1 + \mathbf{b}\cdot\mathbf{B}$ the total perturbed pressure. The final ideal MHD eigenmode equations are cast into the following form:

$$\nabla\psi\cdot\nabla\begin{pmatrix}P_1\\ \xi_\psi\end{pmatrix} = C\begin{pmatrix}P_1\\ \xi_\psi\end{pmatrix} + D\begin{pmatrix}\xi_s\\ \nabla\cdot\xi\end{pmatrix} \tag{7}$$

and

$$E\begin{pmatrix}\xi_s\\ \nabla\cdot\xi\end{pmatrix} = F\begin{pmatrix}P_1\\ \xi_\psi\end{pmatrix}, \tag{8}$$

where $C$, $D$, $E$, $F$ are $2\times2$ matrix operators involving only surface derivatives $\mathbf{B}\cdot\nabla$ and $(\mathbf{B}\times\nabla\psi)\cdot\nabla$. The matrix operators are given by

$$\begin{aligned}
&C_{11} = K_\psi\,,\\
&C_{12} = \omega^2\rho + P'K_\psi + |\nabla\psi|^2\mathbf{B}\cdot\nabla[|\nabla\psi|^{-2}\mathbf{B}\cdot\nabla]\\
&\qquad + (\mathbf{B}\cdot\mathbf{J} - \hat{S}|\nabla\psi|^2)(\hat{S}|\nabla\psi|^2/B^2),\\
&C_{21} = 0,\quad C_{22} = -|\nabla\psi|^2\nabla\cdot(\nabla\psi/|\nabla\psi|^2),\\
&D_{11} = (|\nabla\psi|^2\hat{S} - \mathbf{B}\cdot\mathbf{J})\,(|\nabla\psi|^2/B^2)\mathbf{B}\cdot\nabla,\\
&D_{12} = \gamma_s PK_\psi,\quad D_{21} = |\nabla\psi|^2[K_s - (\mathbf{B}\times\nabla\psi)/B^2\cdot\nabla],\\
&D_{22} = |\nabla\psi|^2\left[1 + \frac{\gamma_s P}{\omega^2\rho}\mathbf{B}\cdot\nabla\left(\frac{\mathbf{B}\cdot\nabla}{B^2}\right)\right],\\
&E_{11} = \frac{\omega^2\rho|\nabla\psi|^2}{B^2} + \mathbf{B}\cdot\nabla\left(\frac{|\nabla\psi|^2\mathbf{B}\cdot\nabla}{B^2}\right),\\
&E_{12} = \gamma_s PK_s,\quad E_{21} = K_s,\\
&E_{22} = \frac{\gamma_s P + B^2}{B^2} + \frac{\gamma_s P}{\omega^2\rho}\mathbf{B}\cdot\nabla\left(\frac{\mathbf{B}\cdot\nabla}{B^2}\right),\\
&F_{11} = -K_s + (\mathbf{B}\times\nabla\psi)/B^2\cdot\nabla,\\
&F_{12} = \mathbf{B}\cdot\nabla(|\nabla\psi|^2/B^2)\hat{S} - [(\mathbf{J}\cdot\mathbf{B})/B^2]\mathbf{B}\cdot\nabla\\
&\qquad - P'K_s,\\
&F_{21} = -1/B^2,\quad F_{22} = -K_\psi/|\nabla\psi|^2,
\end{aligned} \tag{9}$$

where $K_\psi = 2\mathbf{K}\cdot\nabla\psi$, $K_s = 2\,\mathbf{K}\cdot(\mathbf{B}\times\nabla\psi/B^2)$, $\mathbf{K} = (\mathbf{B}/B)\cdot\nabla(\mathbf{B}/B)$ is the curvature,

$$\hat{S} = (\mathbf{B}\times\nabla\psi/|\nabla\psi|^2)\cdot\nabla\times[(\mathbf{B}\times\nabla\psi)/|\nabla\psi|^2]$$

is the negative local magnetic shear. The differential operator $\mathbf{B}\cdot\nabla$ in Eq. (9) operates through on the perturbation. Equations (7) and (8) represent the toroidal generalization of the set of eigenmode equations derived by Appert *et al.*[7] for the circular cylindrical pinch. The boundary condition at the magnetic axis is $\xi_\psi = 0$. For fixed boundary modes the boundary condition is $\xi_\psi = 0$ at the plasma–wall interface. For free boundary modes the boundary condition at the plasma–vacuum interface is given by $\mathbf{b}_v\cdot\nabla\psi = \mathbf{B}\cdot\nabla\xi_\psi$, where the perturbed vacuum magnetic field is $\mathbf{b}_v = \nabla\Phi$ and $\Phi$ is the scalar magnetic potential obtained from the vacuum solution of $\nabla^2\Phi = 0$.

For a given equilibrium, we first solve $\xi_s$ and $\nabla\cdot\xi$ in terms of $P_1$ and $\xi_\psi$ from Eq. (8) by inverting the surface matrix operator $E$. Equation (7) then reduces to an equation for $P_1$ and $\xi_\psi$. Admissible regular solutions must be periodic in both $\theta$ and $\zeta$ directions, and satisfy the appropriate boundary conditions. This procedure fails if the inverse of the surface operator $E$ does not exist for a given $\omega$ at a certain $\psi_0$ surface. Then, Eq. (7) has a radial singularity and nonsquare-integrable solutions with spatial singularity[1–7] at the singular surface $\psi_0$ are possible. If, at each surface, nontrival single-valued periodic solutions in $\theta$ and $\zeta$ can be found for the equation

$$E\begin{pmatrix}\xi_s\\ \nabla\cdot\xi\end{pmatrix} = 0, \tag{10}$$

then the corresponding set of eigenvalues $\omega^2$ forms the continuous spectrum[1–7] for the equilibrium. Equation (10) represents the coupling of the sound branch and the shear Alfvén branch through the curvature and plasma pressure.

## III. BREAKUP OF THE CONTINUOUS SPECTRUM

Since $\zeta$ is an ignorable coordinate for axisymmetric equilibria, we consider the perturbed quantities in the form

$$\xi(\theta,\zeta) = \xi_0(\theta)e^{-in\zeta}\,. \tag{11}$$

Then, we have

$$\begin{aligned}
\mathbf{B}\cdot\nabla\xi &= \mathscr{J}^{-1}\left[\left(\frac{\partial}{\partial\theta} - inq\right)\xi_0\right]e^{-in\zeta}\\
&= \mathscr{J}^{-1}e^{inq\theta}\frac{\partial}{\partial\theta}(\xi e^{-inq\theta}),
\end{aligned} \tag{12}$$

where the Jacobian $\mathscr{J} = (\nabla\psi\times\nabla\theta\cdot\nabla\zeta)^{-1}$, and Eq. (10) reduces to

$$\frac{\omega^2\rho|\nabla\psi|^2}{B^2}Y_1 + \frac{1}{\mathscr{J}}\frac{\partial}{\partial\theta}\left(\frac{|\nabla\psi|^2}{B^2\mathscr{J}}\frac{\partial}{\partial\theta}Y_1\right) + \gamma_s PK_s Y_2 = 0, \tag{13a}$$

$$K_s Y_1 + \left(\frac{\gamma_s P + B^2}{B^2}\right)Y_2 + \frac{\gamma_s P}{\omega^2\rho\mathscr{J}}\frac{\partial}{\partial\theta}\left(\frac{1}{B^2\mathscr{J}}\frac{\partial}{\partial\theta}Y_2\right) = 0, \tag{13b}$$

where $Y_1(\theta) = \xi_s\exp[in(\zeta - q\theta)]$, $Y_2(\theta) = (\nabla\cdot\xi)\exp[in(\zeta - q\theta)]$. Because the coefficients of Eq. (13) are periodic in $\theta$, then from the Floquet theorem the solutions of $Y_1$ and $Y_2$ can be written as

$$Y_1(\theta) = \exp(i\alpha\theta)\tilde{Y}_1(\theta), \tag{14}$$

where $\tilde{Y}_1$ is periodic in $\theta$ with a period of $2\pi$. Since $\xi_s$ and $\nabla\cdot\xi$ are periodic in $\theta$, we must have $\alpha = l - nq$, where $l$ is an integer.

Equation (13) is Hermitian and can be solved by developing a variational principle with the Lagrangian functional given by

$$\begin{aligned}
\mathscr{L} = \oint\Bigg\{\mathscr{J}\omega^2\rho\left(\frac{|\nabla\psi|^2}{B^2}|Y_1|^2 + B^2|Z|^2\right) - \left[\frac{|\nabla\psi|^2}{\mathscr{J}B^2}\left|\frac{\partial Y_1}{\partial\theta}\right|^2\right.\\
\left.+\left(\frac{\mathscr{J}\gamma_s PB^2}{\gamma_s P + B^2}\right)\left|K_s Y_1 - \frac{1}{\mathscr{J}}\left(\frac{\partial Z}{\partial\theta}\right)\right|^2\right]\Bigg\}d\theta,
\end{aligned} \tag{15}$$

where $Z = \gamma_s P(\partial Y_2/\partial\theta)/(\mathscr{J}\omega^2\rho B^2)$. It is straightforward to verify that Eq. (13) is a consequence of the requirement that the functional $\mathscr{L}$ be stationary. The determination of the spectrum reduces to that of finding the eigenvalues $\omega$ and eigenfunctions $Y_1$ and $Y_2$ so that the Lagrangian functional $\mathscr{L}$ is stationary with respect to variations of $Y_1$ and $Y_2$. The

admissible variational functions must be square-integrable and satisfy the periodicity constraint given by Eq. (14).

To proceed, we will adopt the Galerkin procedure where the trial functions depend linearly on certain variational parameters, and the problem is reduced to the minimization of an algebraic quadratic form with these variational parameters.

In terms of Eq. (14), we introduced the Fourier expansion of the perturbations

$$\begin{pmatrix} Y_1 \\ Z \end{pmatrix} = \sum_m \begin{pmatrix} a_m \\ ib_m \end{pmatrix} \exp[i(l+m-nq)\theta] \tag{16}$$

into Eq. (15). Then the variational calculation is equivalent to the determination of eigenvalues and eigenfunctions of the matrix eigenvalue problem

$$\Sigma_{m,m'} (a_{m'} b_{m'})^* L_{m'm} \begin{pmatrix} a_m \\ b_m \end{pmatrix} = 0 , \tag{17}$$

where

$$L_{m'm} = \oint d\theta \begin{pmatrix} A_{11} & A_{12} \\ A_{21} & A_{22} \end{pmatrix} \exp[i(m-m')\theta] , \tag{18}$$

$$A_{11} = \mathcal{J}\omega^2\rho\frac{|\nabla\psi|^2}{B^2} - \frac{\mathcal{J}\gamma_s P B^2 K_s^2}{\gamma_s P + B^2} - \frac{|\nabla\psi|^2}{\mathcal{J}B^2}(l+m-nq)(l+m'-nq) ,$$

$$A_{12} = [-\gamma_s P B^2 K_s/(\gamma_s P + B^2)](l+m'-nq) ,$$

$$A_{21} = [-\gamma_s P B^2 K_s/(\gamma_s P + B^2)](l+m-nq) ,$$

$$A_{22} = \mathcal{J}\omega^2\rho B^2 - [\gamma_s P B^2/\mathcal{J}(\gamma_s P + B^2)] \times (l+m-nq)(l+m'-nq) .$$

In the following we will let $l = 0$ without the loss of generality.

From Eq. (17), a numerical solution of the continuous spectrum for a low-$\beta$ circular, numerical equilibrium is shown in Fig. 1, where the eigenvalues $(\omega/\omega_A)^2$ are plotted versus the $\psi$ surface for an $n = 1$ perturbation. The normalization frequency is defined by $\omega_A = V_A(0)/q(a)R$. The numerical equilibrium has an aspect ratio $R/a = 4$, average beta $\beta_{av} = 0.04\%$, $q(0) = 1.0408$, and $q(a) = 2.3$. The broken curves represent the continuous spectra for $m = 1$ and $m = 2$ modes in the absence of toroidal couplings, and they cross at the $q = 1.5$ surface. Because of the nonuniformity of the toroidal magnetic field, coupling of different poloidal harmonics results in the breakup of the continuous spectra (solid curves). The continuum gaps are located at $q(r_0) = (m_1 + m_2)/2n$ surfaces with corresponding local shear Alfvén frequencies $\omega_0^2 = [(m_1 - m_2)V_A(r_0)/2q(r_0)R]^2$, where $m_1$ and $m_2$ are two different poloidal mode numbers. As shown in Fig. 1, the gap size is of the order of $(r_0/R)$ with $m_1$ and $m_2$ differing by one. When $m_1$ and $m_2$ differ by more than one, the gap size is of the order $(r_0/R)^2$.

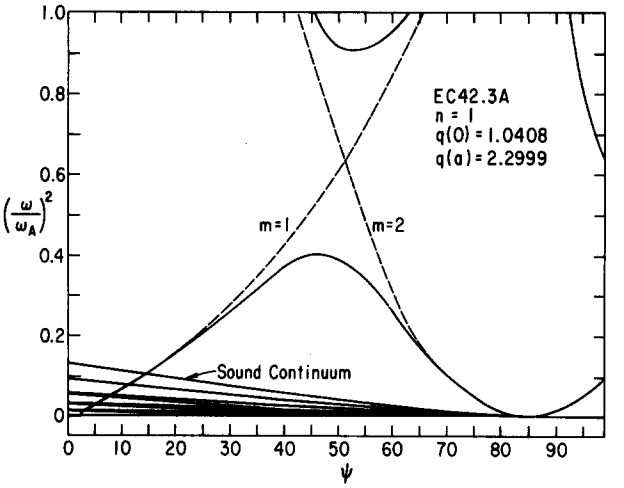


FIG. 1. The shear Alfvén continous spectrum with gaps for a low-$\beta$ toroidal equilibrium with $n = 1$, $\beta_{av} = 0.04\%$, $R/a = 4$, $q(0) = 1.0408$, and $q(a) = 2.3$. The uncoupled spectra (dotted line) of $m = 1$ and $m = 2$ cross at the $q = 1.5$ surface. The sound continuum is also shown.

To obtain the shear Alfvén continuous spectrum as a result of the toroidal coupling effects, we employ a large aspect ratio, low-$\beta$ equilibrium derived by Greene *et al.*[13] Considering $P \sim \epsilon^2$, $q \sim 1 + \epsilon^2 q^{(2)}$, the flux surfaces of up–down symmetric equilibrium can be expressed by

$$X = R - \epsilon r\cos\theta - \epsilon^2\Delta(r) + \epsilon^3[E(r) + G(r)]\cos\theta + \cdots , \tag{19a}$$

$$Z = \epsilon r\sin\theta + \epsilon^3[E(r) - G(r)]\sin\theta + \cdots , \tag{19b}$$

where $\epsilon$ is a tag denoting the small ordering parameter which is set to one, $r$ labels the flux surface, $\theta$ is the poloidal angle, $\Delta(r)$ measures the shift of the center of the surfaces from the magnetic axis, $E(r)$ determines the ellipticity of the surfaces, and $G(r)$ modifies the labeling of the surfaces. Then in an $\epsilon$ expansion, we have

$$\mathcal{J} = \alpha(r)[1 + 2\epsilon\sigma(r)\cos\theta + O(\epsilon^2)] , \tag{20a}$$

$$\frac{|\nabla\psi|^2}{B^2} = \frac{\epsilon^2 G(r)}{B_0^2}\left[1 + 2\epsilon\left(\frac{r}{R} + \Delta'\right)\cos\theta + O(\epsilon^2)\right] , \tag{20b}$$

where $\Delta' = d\Delta(r)/dr$. The term involving $\sigma$ in $\mathcal{J}$ will subsequently cancel. From Eq. (18) we find that to order $\epsilon$ the shear Alfvén waves decouple from the sound waves. Concentrating on the shear Alfvén branch, Eq. (17) reduces to

$$\frac{2\pi\epsilon^2 G(r)}{\alpha(r)B_0^2}\sum_{m,m'}\left\{\Omega^2\left[\delta_{m,m'} + \epsilon\left(\frac{r}{R} + \Delta' + \sigma\right)(\delta_{m,m'-1} + \delta_{m,m'+1})\right] - (m-nq)(m'-nq)\left[\delta_{m,m'} + \epsilon\left(\frac{r}{R} + \Delta' - \sigma\right)(\delta_{m,m'-1} + \delta_{m,m'+1})\right] + O(\epsilon^2)\right\} a_m a_{m'}^* = 0 , \tag{21}$$

where $\Omega^2 = \omega^2\rho\alpha^2(r)$, $\delta_{m,m'}$ is the Kronecker delta. To $O(\epsilon)$ only the couplings of neighboring poloidal harmonics are present. Couplings of poloidal harmonics with $m$ differing more than one come in $O(\epsilon^2)$ terms, which are neglected in Eq.

(21). Now keeping only $m$ and $m+1$ modes, we have the dispersion relation

$$\begin{vmatrix} (\Omega^2-\Omega_0^2) & \epsilon[(r/R+\Delta'+\sigma)\Omega^2-(r/R+\Delta'-\sigma)\Omega_0\Omega_1] \\ \epsilon[(r/R+\Delta'+\sigma)\Omega^2-(r/R+\Delta'-\sigma)\Omega_0\Omega_1] & (\Omega^2-\Omega_1^2) \end{vmatrix} = 0, \tag{22}$$

where $\Omega_0=(m-nq)$, $\Omega_1=(m+1-nq)$. Near the crossing surfaces of $\Omega_0^2$ and $\Omega_1^2$ where $|\Omega_0^2-\Omega_1^2|\leqslant 0(\epsilon^2)$, we have $\Omega_0\simeq-\Omega_1$ and $\Omega_0^2\simeq(1/4)$. Then the eigenvalue $\Omega^2$ is approximately given by

$$\Omega_\pm^2=\Omega_0^2[1\pm 2\epsilon(r/R+\Delta')+O(\epsilon^2)], \tag{23}$$

which is independent of $m$ and $n$, and the toroidicity comes through $|\nabla\psi|^2/B^2$ only. It is clear from Eq. (22) that when $|\Omega_0^2-\Omega_1^2|\gtrsim O(1)$, the solutions of $\Omega^2$ are the uncoupled ones plus corrections of $O(\epsilon^2)$. The eigenfunctions $Y_\pm$ corresponding to the eigenfrequencies $\Omega_\pm^2$ can be easily obtained from Eq. (21) and are given by

$$Y_-(\theta)=\exp[i(m+\tfrac{1}{2}-nq)\theta]\cos(\theta/2)$$

and

$$Y_+(\theta)=i\exp[i(m+\tfrac{1}{2}-nq)\theta]\sin(\theta/2). \tag{24}$$

The wave corresponding to the lower frequency $\Omega_-$ is localized in the outside of the torus $\theta=0$, where the curvature is bad. The wave with the higher frequency $\Omega_+$ is localized in the good curvature region at $\theta=\pi$.

Physically, the gap in the continuous spectrum is analogous to the gap that appears in the energy spectrum of valence electrons in a periodic potential well of the crystal lattice.[14] The gaps in the electron energy spectrum occur because Bragg reflection of a traveling electron wave off the lattice ions results in standing electron waves, which are either localized in the well between the ions (lower energy state) or at the top of the well near the ions (higher energy state). For the shear Alfvén waves, the gaps appear because of the periodic variation of the magnetic field which induces coupling of poloidal harmonics, and the waves are localized in the good or bad curvature regions. This can be demonstrated from Eq. (13a) by letting $P=0$, and we have

$$\frac{d^2Y_1}{d\theta^2}+\omega^2\rho\frac{|\nabla\psi|^4}{B^4}Y_1=0, \tag{25}$$

where we have chosen $\mathscr{J}=|\nabla\psi|^2/B^2$, which does not affect our results, because to $O(\epsilon)$ the gaps should be independent of the choice of $\mathscr{J}$. Equation (25) reduces to the Mathieu equation[15] in the large-aspect-ratio limit

$$\frac{d^2}{d\theta^2}Y_1+\Omega^2\left[1+4\epsilon\left(\frac{r}{R}+\Delta'\right)\cos\theta\right]Y_1=0, \tag{26}$$

which admits an infinite set of characteristic values $\Omega^2$. These infinite pairs of characteristic values correspond to periodic solutions of $Y_1$ and define the gaps between the bands of continuous spectra located at $\Omega^2=(l/2)^2$, $l=1,2,\ldots$. The lowest characteristic pairs that define the gaps are given by Eq. (23) to $O(\epsilon)$. For $\Omega^2$ inside the gaps, $Y_1$ is divergent at large $\theta$. It is also straightforward to show from Eq. (26) that for the higher frequency gaps, the gap sizes are of $O(\epsilon^2)$.

## IV. LOW-$n$ TOROIDICITY-INDUCED GLOBAL SHEAR ALFVÉN MODES

In this section we show that the toroidal coupling effects due to a nonuniform magnetic field can induce discrete, global shear Alfvén eigenmodes with frequencies inside the continuum gap. Direct analysis of the ideal MHD eigenmode equations, Eqs. (7) and (8), is extremely complicated even in the large-aspect-ratio limit. Instead, we employ the reduced MHD equations introduced by Izzo *et al.*[16] to obtain analytical solutions of the toroidicity-induced shear Alfvén eigenmodes. In a large-aspect-ratio, zero-$\beta$ tokamak, the linearized, reduced MHD equation describing shear Alfvén waves is given by

$$\mathbf{B}\cdot\nabla[\Delta^*(X^2\mathbf{B}\cdot\nabla u)]+\omega^2\rho X^2\nabla_\perp^2 u=0, \tag{27}$$

where

$$\Delta^*=X\frac{\partial}{\partial X}\frac{1}{X}\frac{\partial}{\partial X}+\frac{\partial^2}{\partial z^2},\quad \nabla_\perp^2=\nabla^2-\left(\frac{\mathbf{B}}{B}\right)\cdot\nabla\left(\frac{\mathbf{B}}{B}\cdot\nabla\right),$$

$\rho$ is the plasma mass density, $\rho X^2$ is assumed to be constant, and $u$ is the velocity stream function. Equation (27)[16] is derived from the linearized ideal MHD equations (4)–(6), and is correct up to the order of $\epsilon$. Consider an equilibrium with circular, concentric magnetic surfaces and we have $\mathbf{B}=(I_0/X)[\hat{\zeta}+(r/qX)\hat{\theta}]$, where $X=R[1+(r/R)\cos\theta]$, $R$ is the major radius, $r$ is the minor radius, $\theta$ is the poloidal angle, and $\zeta$ is the toroidal angle. The velocity stream function $u$ can be expanded as

$$u=\sum_m u_m\exp[i(m\theta-n\zeta)].$$

Then to $O(\epsilon)$, Eq. (27) reduces to

$$4q_0^2(n-m/q)\nabla_\perp^2[(n-m/q)u_m]-\Omega^2\nabla_\perp^2 u_m = \hat{\epsilon}\Omega^2\nabla_\perp^2(u_{m+1}+u_{m-1}), \tag{28}$$

where $\Delta^*\simeq\Delta_1^2$ is assumed, $\hat{\epsilon}$ is of the order of $r/R$ and contains all $(r/R)$ contributions to this order, $\Omega^2=4\omega^2/\omega_A^2,\omega_A^2=(B_0^2/\rho q_0^2R^2)$, $B_0=I_0/R$, $q_0=q(r_0)=(m+\frac{1}{2})/n$ is the safety factor at the crossing surface of the local Alfvén frequencies for the $m$ and $(m+1)$ modes, and $\rho$ is assumed to be constant. To solve Eq. (28), we consider the region $q$ around $q_0$ so that $(n-m/q)\simeq(1+2\,msx)/2q_0$, where $s=r_0q_0'/q_0$, $x=(r-r_0)/r_0<1$. Further assuming that $\nabla_\perp^2u_m\simeq[(\partial^2/\partial r^2)-(m^2/r^2)]u_m$, Eq. (28) for the $m$th harmonic then reduces to

$$\begin{aligned}&(1+2msx)\left(\frac{d^2}{dx^2}-m^2\right)(1+2msx)u_m \\ &\quad-\Omega^2\left(\frac{d^2}{dx^2}-m^2\right)u_m \\ &\quad=\hat{\epsilon}\Omega^2\left[\left(\frac{d^2}{dx^2}-(m+1)^2\right)u_{m+1}\right. \\ &\qquad\left.+\left(\frac{d^2}{dx^2}-(m-1)^2\right)u_{m-1}\right].\end{aligned} \tag{29}$$

To $O(\hat{\epsilon})$, Eq. (29) can be truncated to retain only $m$ and $(m+1)$ harmonics and we form a closed set of equations

$$\left[\frac{d}{dy}[(1+2my)^2-\Omega^2]\frac{d}{dy} - \left(\frac{m}{s}\right)^2[(1+2my)^2-\Omega^2]\right]u_m = \hat{\epsilon}\Omega^2\left[\frac{d^2}{dy^2}-\left(\frac{m+1}{s}\right)^2\right]u_{m+1} \tag{30a}$$

and

$$\left[\frac{d}{dy}\{[1-2(m+1)y]^2-\Omega^2\}\frac{d}{dy} - \left(\frac{m+1}{s}\right)^2 \times\{[1-2(m+1)y]^2-\Omega^2\}\right]u_{m+1} = \hat{\epsilon}\Omega^2\left[\frac{d^2}{dy^2}-\left(\frac{m}{s}\right)^2\right]u_m , \tag{30b}$$

where $y = sx$.

Equation (30) can be solved by the method of asymptotic matching by considering two regions of $y$: (*i*) $y\sim\hat{\epsilon}$ and (*ii*) $y\sim\hat{\epsilon}^{1/2}$. Taking $(1-\Omega^2)\sim O(\hat{\epsilon})$ and $s\sim m \sim (u_m/u_{m+1})\sim O(1)$, then in these regions Eq. (30) reduces to

$$\frac{d}{dy}(1-\Omega^2+4my)\frac{d}{dy}u_m = \hat{\epsilon}\Omega^2\frac{d^2}{dy^2}u_{m+1} , \tag{31a}$$

$$\frac{d}{dy}[1-\Omega^2-4(m+1)y]\frac{d}{dy}u_{m+1} = \hat{\epsilon}\Omega^2\frac{d^2}{dy^2}u_m , \tag{31b}$$

in the $y\sim O(\hat{\epsilon})$ region, and to

$$\frac{d}{dy}y\frac{d}{dy}\begin{pmatrix}u_m\\u_{m+1}\end{pmatrix} = 0, \tag{32}$$

in the $y\sim(\hat{\epsilon}^{1/2})$ region. The solutions in the $y\sim O(\hat{\epsilon})$ region are given by

$$u_m = C_0\left[\frac{1}{2}\ln[(y+a)^2+b^2] - \frac{a}{b}\tan^{-1}\left(\frac{y+a}{b}\right)\right] + C_1\left[\frac{1}{b}\tan^{-1}\left(\frac{y+a}{b}\right)\right], \tag{33a}$$

$$u_{m+1} = \hat{C}_0\left[\frac{1}{2}\ln[(y+a)^2+b^2] - \frac{a}{b}\tan^{-1}\left(\frac{y+a}{b}\right)\right] + \hat{C}_1\left[\frac{1}{b}\tan^{-1}\left(\frac{y+a}{b}\right)\right], \tag{33b}$$

where the integration constants are defined by

$$\frac{\hat{C}_1}{\hat{C}_0} = \frac{4m(a^2+b^2)-(1-\Omega^2)(C_1/C_0)}{8ma-(1-\Omega^2)-4m(C_1/C_0)},$$

$$\hat{\epsilon}\Omega^2\hat{C}_0 = 4mC_1+(1-\Omega^2-8ma)C_0 ,$$

$$a = (1-\Omega^2)/8m(m+1)\sim O(\hat{\epsilon}) ,$$

and

$$b^2 = \frac{\{\hat{\epsilon}^2\Omega^4-(1-\Omega^2)^2[1+1/4m(m+1)]\}}{16m(m+1)}\sim O(\hat{\epsilon}) .$$

The solutions in the $y\sim\hat{\epsilon}^{1/2}$ region are given by

$$u_m = a_1(\ln|y|+b_1) \tag{34a}$$

and

$$u_{m+1} = a_2(\ln|y|+b_2) , \tag{34b}$$

where $a_1$, $a_2$, $b_1$, and $b_2$ are real finite integration constants of $O(1)$. Here $b_1$ and $b_2$ are determined by matching the solutions to those of Eq. (28) in the $y\sim O(1)$ region, which depend on the safety factor $q(r)$ (or shear). We do not pursue the $y\sim O(1)$ solutions of Eq. (28), but instead, assume that $b_1$ and $b_2$ are known constants. Then we obtain a dispersion relation by matching the solutions in the $y\sim O(\hat{\epsilon})$ region, Eq. (33), to those in the $y\sim O(\hat{\epsilon}^{1/2})$ region, Eq. (34). The dispersion relation depends on $b_1$ and $b_2$ and is given by

$$b = (2m+1)(1-\Omega^2)\alpha/8m(m+1) , \tag{35}$$

where

$$\alpha = 2(b_1-b_2)/[\pi(1+b_1b_2/\pi^2)] .$$

In general, $\alpha$ is real and finite, and we must require $b^2>0$ so that the $y\sim O(\hat{\epsilon})$ solutions, Eqs. (33a) and (33b), are regular. The corresponding eigenfrequencies are given by

$$\Omega^2\simeq(1\pm\hat{\epsilon}h)+O(\hat{\epsilon}^2) , \tag{36}$$

where

$$h^2 = 4m(m+1)/[1+4m(m+1)+(2m+1)^2\alpha^2]>0 .$$

Since $h^2<1$, $\Omega^2$ is inside the continuum gap, defined by $\Omega^2=1\pm\hat{\epsilon}$, and depends on the shear [or $q(r)$] and boundary conditions through $b_1$ and $b_2$. Thus, we have shown that for any given regular $y\sim 0(1)$ solutions, i.e., given finite $b_1$ and $b_2$, we can always obtain regular global solutions with discrete eigenvalues $\Omega^2$ lying inside the continuum gap due to the coupling of $m$ and $(m+1)$ poloidal harmonics. In the high-$m$ limit, $h^2\to 1$ since $b_1\to b_2$, and $\Omega^2$ is independent of $n$ and $m$.

Figure 2 shows the poloidal harmonics of the eigenfunction $\xi_\psi$ vs $\sqrt{\psi}$ for the same equilibrium as used in Fig. 1. The eigenfrequency for this fixed boundary $n=1$ mode is $(\omega/$

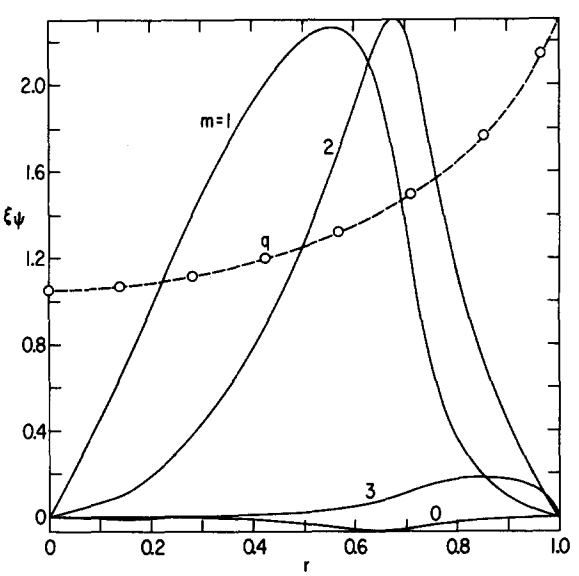


FIG. 2. The poloidal harmonics of the fixed boundary $n=1$ toroidicity-induced shear Alfvén eigenmode $\xi_\psi$ vs $r$ ($r=\sqrt{\psi}$) for the same equilibrium as in Fig. 1. The eigenfunction is primarily the $m=1$ and $m=2$ components because $q(r)$ varies from $q(0)=1.0408$ to $q(a)=2.3$ as shown.

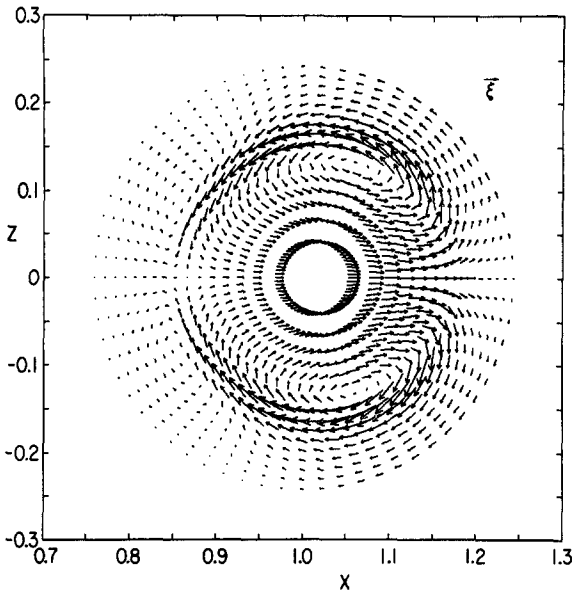


FIG. 3. Poloidal projection of the displacement vector, $\xi$, for the $n = 1$ fixed boundary toroidicity-induced shear Alfvén eigenmode as shown in Fig. 2.

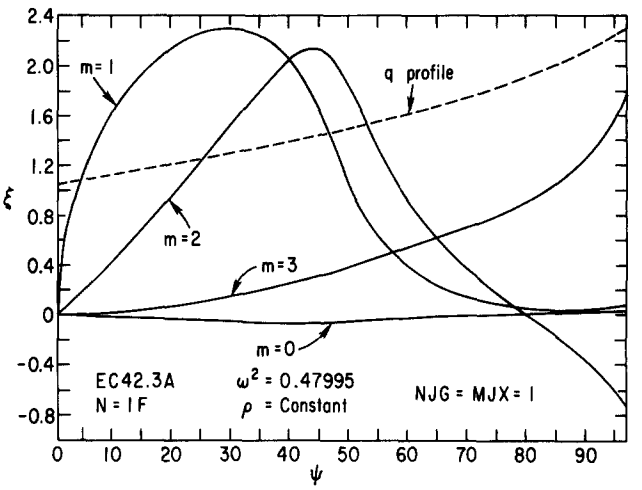


FIG. 4. The poloidal harmonics of the free boundary $n = 1$ toroidicity-induced shear Alfvén eigenmode $\xi_\psi$ vs $\psi$ for the same equilibrium as in Fig. 1. The $q(\psi)$ profile is also shown.

$\omega_A)^2 = 0.5$. The solution is obtained by numerically integrating Eqs. (7) and (8) by employing a nonvariational code (NOVA).[17] The NOVA code employs cubic $B$ spline finite elements and Fourier expansion in a general flux coordinate $(\psi,\theta,\zeta)$ system and has been extensively compared with the PEST code.[18] The $q(\psi)$ profile is also shown in Fig. 2. It is clear from Fig. 2 that primarily the $m = 1$ and 2 harmonics dominate around the $q = 1.5$ surface with a small coupling to $m = 3$ harmonic towards the plasma surface. Projection of the displacement vector $\xi$ on the $\phi = 0$ plane is shown in Fig. 3 where the plasma vortices corresponding to $m = 1$ and 2 harmonics are clearly seen. Figure 4 shows the eigenfunction $\xi_\psi$ vs $\psi$ for the $n = 1$ free boundary mode for the same equilibrium with the eigenfrequency $(\omega/\omega_A)^2 = 0.48$. This result clearly supports our analytical analysis that boundary conditions only modify the eigenfrequency slightly through $\alpha^2$ (i.e., $b_1$ and $b_2$). Numerical solutions of higher $n$ modes ($n \geqslant 2$) have also been obtained with frequencies inside the lowest continuum gap. The results also indicate that the number of the discrete, global toroidicity-induced shear Alfvén mode is proportional to $n$ for a given $q(r)$ profile. As $n$ becomes large, the discrete spectra fill up the continuum gap.

The discrete toroidicity-induced shear Alfvén modes have been obtained previously in the infinite $n$ limit.[10] The shear Alfvén eigenmode equation for a low-$\beta$ plasma with circular, concentric magnetic surfaces obtained by employing the high-$n$ WKB-ballooning formalism is given by

$$\left(\frac{d^2}{d\theta^2} + \Omega^2(1 + 2\epsilon\cos\theta) - \frac{s^2}{(1 + s^2\theta^2)^2}\right)\Phi = 0, \tag{37}$$

where $s = rq'/q$ is the shear, $\epsilon = 2r/R$, $\Phi = (1 + s^2\theta^2)^{1/2}\hat{\phi}$, $\hat{\phi}$ is the electrostatic potential. Equation (37) has been analyzed for the toroidicity-induced shear Alfvén modes by a two-scale analysis and asymptotic matching. The eigenfrequency of the even parity mode in the lowest continuum gap is given by

$$\Omega^2 = \tfrac{1}{4}[1 + \epsilon(1 - s^2\pi^2/8)]^{-1} \tag{38}$$

for $s^2 \ll 1$, and for $s^2 \gg 1$ we have

$$\Omega^2 = \tfrac{1}{4}[1 - \epsilon(1 - \pi^2/72s^4)]^{-1}. \tag{39}$$

From Eqs. (38) and (39), we see that as $s \to 0$, $\Omega^2$ approaches the lower end of the gap, and as $s \to \infty$, $\Omega^2$ goes to the upper end of the gap. The odd parity solution is nonexistent. Note that Eq. (37) admits only one degenerate solution. This degeneracy is due to the lowest-order ballooning formalism which ignores the equilibrium radial variations.

## V. DISCUSSION

In this paper, we have studied low-$n$ shear Alfvén waves in axisymmetric toroidal plasmas. We have shown that the toroidal coupling effects due to a nonuniform magnetic field over a magnetic surface not only break up the shear Alfvén continuous spectrum, but also result in discrete global toroidicity-induced shear Alfvén eigenmodes with frequencies inside the continuum gaps. The understanding of the shear Alfvén continuous spectra in axisymmetric toroidal plasmas is essential for Alfvén resonance heating and mode conversion, which crucially depend on the location of the singular surface. The low-$n$ toroidicity-induced shear Alfvén eigenmodes may be more efficiently applied to wave heating and current drive due to its global eigenmode structure. Unlike the Alfvén resonance heating which involves localized perturbations at the singular surface with the parallel phase speed $\omega/k_\parallel = V_A$, the global toroidicity-induced shear Alfvén modes involve several poloidal harmonics so that parallel phase speed $\omega/k_\parallel$ can be either greater or smaller than $V_A$ at different radial locations and, therefore, both electron and ion Landau dampings can be substantially stronger globally.

Another application of toroidicity-induced shear Alfvén modes concerns instabilities induced by energetic particles. In neutral beam injection experiments in PLT and PDX,[19] high frequency oscillations ($f \approx 100$ kHz) have been observed in Mirnov coils and soft x-ray signals. These

oscillations are dominantly $m = n \approx 4$–10 and occur near the $q = 1$ surface where beam particles are highly concentrated. Our numerical calculations indicate that toroidicity-induced shear Alfvén modes can be destabilized by beam particle magnetic drift resonances and may account for these experimental observations. In thermonuclear fusion regimes, energetic $\alpha$ particles are produced in large amounts. Their interactions with toroidicity-induced shear Alfvén modes may lead to serious instabilities and should, therefore, be investigated.

## ACKNOWLEDGMENT

This work was supported by United States Department of Energy Contract No. DE-AC02-76-CHO-3073.

[1]Z. Sedlacek, J. Plasma Phys. **5**, 239 (1971); E. M. Barston, Ann. Phys. (NY) **29**, 282 (1964).
[2]H. Grad, Phys. Today **22**, 34 (1969).
[3]J. Tataronis and W. Grossman, Z. Phys. **14**, 203 (1973); L. Chen and A. Hasegawa, J. Geophys. Res. **79**, 1033 (1974); C. Uberoi, Phys. Fluids **15**, 1673 (1972).
[4]R. L. Dewar, R. C. Grimm, J. L. Johnson, E. A. Frieman, J. M. Greene, and P. H. Rutherford, Phys. Fluids **17**, 930 (1974); M. S. Chance, J. M. Greene, R. C. Grimm, and J. L. Johnson, Nucl. Fusion **17**, 65 (1977).
[5]Y. P. Pao, Nucl. Fusion **15**, 631 (1975).
[6]E. Hameiri, Commun. Pure Appl. Math. **38**, 43 (1985); J. P. Goedbloed, Phys. Fluids **18**, 1258 (1975).
[7]K. Appert, R. Gruber, and J. Vaclavik, Phys. Fluids **17**, 1471 (1974).
[8]O. P. Pogutse and E. I. Yurchenko, Nucl. Fusion **18**, 1629 (1978); D. A. D'Ippolito and J. P. Goedbloed, Plasma Phys. **22**, 1091 (1980).
[9]C. E. Kieras and J. A. Tataronis, J. Plasma Phys. **28**, 395 (1982).
[10]C. Z. Cheng, L. Chen, and M. S. Chance, Ann. Phys. (NY) **161**, 21 (1984).
[11]K. Appert, R. Gruber, F. Troyon, and J. Vaclavik, Plasma Phys. **24**, 1147 (1982).
[12]S. M. Mahajan, D. W. Ross, and G. L. Chen, Phys. Fluids **26**, 2195 (1983).
[13]J. M. Greene, J. L. Johnson, and K. E. Weimer, Phys. Fluids **14**, 671 (1971).
[14]C. Kittell, *Introduction to Solid State Physics*, 5th ed. (Wiley, New York, 1976).
[15]M. Abramowitz and I. A. Stegun, *Handbook of Mathematical Functions*, (National Bureau of Standards, Washington, D.C., 1964).
[16]R. Izzo, D. A. Monticello, W. Park, J. Manickam, H. R. Strauss, R. C. Grimm, and K. McGuire, Phys. Fluids **26**, 2240 (1983).
[17]C. Z. Cheng and M. S. Chance, submitted to J. Comput. Phys.
[18]R. C. Grimm, J. M. Greene, and J. L. Johnson, Methods Comput. Phys. **16**, 253 (1976).
[19]K. M. McGuire, in *Proceedings of the 1984 International Conference on Plasma Physics*, Lausanne, Switzerland (Commission of the European Communities, Brussels, 1984), Vol. I, p. 123.